

# A spatio-kinematic study of the interaction of the planetary nebula NGC 246 with the interstellar medium

C. Muthu<sup>1</sup>, B.G. Anandarao<sup>1</sup>, and S.R. Pottasch<sup>2</sup>

<sup>1</sup> Physical Research Laboratory, Navrangpura, Ahmedabad, India – 380009 (c.muthu@prl.ernet.in; anand@prl.ernet.in)

<sup>2</sup> Kapteyn Astronomical Institute, Groningen University, Postbus 800, 9700 AV Groningen, The Netherlands (pottasch@astro.rug.nl)

Received 19 February 1999 / Accepted 13 December 1999

**Abstract.** Spatio-Kinematic observations were made on NGC 246 in the [OIII] 5007Å line using an Imaging Fabry-Perot Spectrometer. Evidence for the deceleration effect was found in the leading edge of the nebular shell, possibly due to its interaction with the interstellar medium. Further, we show that the [OIII] electron temperature derived from spectrographic data in the leading half is larger than that in the trailing half possibly due to the compressional heating.

**Key words:** ISM: planetary nebulae: individual: NGC 246 – ISM: kinematics and dynamics

## 1. Introduction

The possibility of interaction between the interstellar medium (ISM) and the planetary nebulae (PNe) with large proper motions was first suggested by Gurzadyan (1969). Such an interaction can occur when the nebular density ( $n_n$ ) drops below a critical value ( $n_{crit}$ ) defined by the ISM density and the nebular relative velocity with respect to the ISM (Borkowski et al. 1990). The nebula can then undergo significant changes in its morphology and physical parameters as well as deceleration in the leading edge in comparison to the trailing edge (Soker et al. 1991). Shell fragmentation under the influence of Rayleigh-Taylor (RT) and Kelvin-Helmholtz (KH) instabilities may occur at the PN-ISM interface. While pioneering theoretical studies have already been made on this issue (Dgani & Soker 1998 and the references therein), there is still a lack of kinematic observational evidence to show the expected effects due to such an interaction (Soker et al. 1991). However, the morphological behaviour of PN-ISM interaction has been studied observationally using CCD images at different wavelengths (Philip & Soker 1990; Tweedy et al. 1995; Hollis et al. 1996; Soker & Zucker 1997).

The planetary nebula NGC 246 (PN G 118.8-74.7; IRAS 00445-1207, Acker et al. 1992) is perhaps the best example which shows noticeable pathologies among the interacting PNe (Soker et al. 1991). Further, the nebula is situated at a high galactic latitude and its distance is known quite accurately (600 pc from Acker et al. 1998 using HIPPARCOS and 500 pc from

Pottasch 1996 using its binary core). The proper motion of the nebula was accurately measured by HIPPARCOS as  $0.023''/yr$  directed towards the west. Using this and the radial velocity of  $-50$  km/s (Schneider et al. 1983), we calculate the space velocity  $V_*$  as 86 km/s. The nebular morphology suggests an oval shaped ring (Chu et al. 1987) with the central star slightly displaced towards the leading edge. The leading half is brighter and has a sharper boundary than the trailing half. The nebular images show an inhomogeneous density structure indicating that it has probably been distorted by the ISM interaction. The available kinematic observations are very limited; they involve either single large spatial sampling (Johnson 1976; Sabbadin et al. 1986) or small spatial sampling confined only to the centre of the nebula (Robinson et al. 1982). It is important to obtain spatially sampled data on large area of the nebula in order to establish kinematic manifestations of the interaction. Further, the ISM interaction may lead in principle to differences in the electron temperature and density in the leading and trailing halves of the nebula. Such an effect in temperature was not detected so far.

We report on new [OIII] 5007 Å line kinematic observations on NGC 246 made by an Imaging Fabry-Perot Spectrometer (IFPS). We report also the electron density and temperature derived from medium resolution spectrographic observations. We discuss these results in relation to the nebular interaction with the ISM and show some evidence for significant differences in the observed parameters between the leading and the trailing halves.

## 2. Observations and data analysis

The kinematic observations were made using the PRL IFPS at the f/13 Cassegrain focus of the 1.2 m telescope at Gurushikhar, Mt. Abu, India during the nights of 20 December 1995 and 13 December 1996 under reasonably good and stable seeing of  $2''$ . The instrumental details may be found in Seema et al. (1992). We used a piezo-electrically scanned and servo-controlled Fabry-Perot etalon (Queensgate, UK) of 50 mm usable aperture and a cavity gap of  $416 \mu\text{m}$  which gives a Free Spectral Range (FSR) of 180 km/s at 5000 Å. For an overall finesse of 16, this gives a velocity resolution width of 12 km/s. The stability of the etalon against possible atmospheric changes

was better than  $0.02\text{\AA}$  during the observations. The detector used in the IFPS is an Imaging Photon Detector (IPD) which has an equivalent pixel size of  $35\ \mu\text{m}$  which when coupled with the IFPS optics gives a net plate scale of  $1''/\text{pix}$ . An interference filter with a bandwidth of  $15\ \text{\AA}$  was used to isolate the [OIII] line at  $5007\ \text{\AA}$ .

Since NGC 246 is rather a faint planetary nebula for a 1.2 m telescope, we needed to integrate for one hour for obtaining a single frame of interferogram at a fixed cavity gap of the etalon to get a good signal to noise ratio (S/N). As it would require prohibitively long observation time to obtain a series of such frames covering more than one FSR (scanning mode, Atherton et al. 1982), we were forced to use the IFPS in the classical spectrographic/interferogram mode (Vaughan 1989). It was possible for us to record two interferograms at two different gap settings of the etalon covering a significant portion of the nebula. The integration time is 3600 sec for the first interferogram (December 1995, frame A) and 5400 sec for the second interferogram (December 1996, frame B). Dark frames of the same duration were taken for each object frame. Two narrow band ( $15\text{\AA}$  FWHM) [OIII] line filtergrams of NGC 246 were also obtained on both the dates under the same conditions in order to relate the emitting regions with the fringes. The overall S/N ratio of these interferograms is between 3.3 to 14.6. The object was guided during the observations using an image intensifier locked on to a reference star to give a tracking accuracy of  $1''$ . Standard calibration interferograms were obtained soon after the observations using the helium line at  $5015\ \text{\AA}$ . The dark-subtracted object frames were then analysed using the standard methods (e.g., Joncas & Roy 1986; Chakraborty & Anandarao 1997) to derive the velocity field on the object. A set of 48 line profiles representing different spatial regions on the nebula were obtained by taking radial scans from the centre of the fringe system across every fringe. Such scans were made with an angular integration of  $20^\circ$  for frame A and  $15^\circ$  for frame B. This corresponds to a spatial integration along the radial direction across a fringe of  $2.2''$  (decided by the overall spatial resolution that includes the seeing and tracking accuracies) and along the circumference of a fringe ranging from  $18.6''$  to  $31''$  for frame A and  $7.9''$  to  $23.8''$  for frame B. The ranges calculated correspond to different spatial locations from the centre to the edge of the interferograms. Thus, the line profiles obtained by radial scans were space-averaged over an area between  $2.2'' \times 17.6''$  to  $2.2'' \times 30.5''$  for frame A and between  $2.2'' \times 7.9''$  to  $2.2'' \times 23.8''$  for frame B. The S/N ratios for these integrated profiles are in the range of 10 – 25.

Each of these line profiles was then processed using a multi-Gaussian fitting code (Anandarao & Rao 1985) to find the constituent Gaussian components. The selection procedure for the best fit excludes the components whose amplitudes are less than 10 % of the maximum signal of the profile and/or whose widths are less than the instrumental width (12 km/s).

The overall velocity resolution is decided by the combined effect of the instrumental velocity resolution (12 km/s) and the velocity dispersions across the effective spatial resolution element ( $2.2''$ ). The spectral dispersion across a pixel varies with

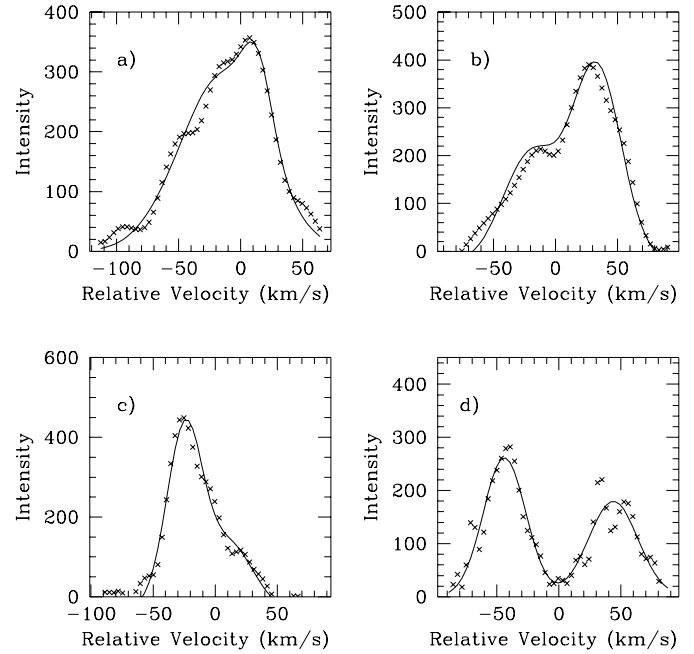


**Fig. 1a–d.** [OIII] Emission line profiles on NGC 246; crosses represent the data and the solid curves refer to the model double-Gaussian fits to the data. The position of these profiles are shown in Fig. 2. The model parameters are listed in Table 1.

the radial distance from the centre of the fringe system by a quadratic relationship. The estimated dispersion across one spatial element at the 30th and the 91st pixels are 9.7 km/s and 29 km/s respectively. These are the values for the two extremities considered in our analysis. in radial velocities) varied between  $\pm 2$  to  $\pm 5$  km/s depending upon the complexity of the profile.

In addition, we obtained service observations on the nebula using the Intermediate Dispersion Spectrograph (IDS) on the 2.5 m Issac Newton Telescope at La Palma during 1997. The spectrographic slit was placed  $10''$  away from the central star towards the leading section at a position angle (PA) of  $45^\circ$  (Fig. 2). The PA had been chosen in order to sample nearly equal lengths of the two sections which was not possible for the ideal case of  $90^\circ$ . Two gratings were used for these observations, viz. the R400B with a dispersion of  $2.3\text{\AA}/\text{pix}$  for  $\lambda\lambda$  3340 $\text{\AA}$  – 4660 $\text{\AA}$  (on 21 August 1997) and the R150V with a dispersion of  $5.97\text{\AA}/\text{pix}$  for  $\lambda\lambda$  3785 $\text{\AA}$  – 7215 $\text{\AA}$  (on 24 September 1997). The data were corrected for bias and flat field using IRAF and the one dimensional spectra were extracted from the task APALL. Then the spectra were calibrated for wavelength using the CuAr lamp spectra and for the flux using the standard star Hiltner 102.

### 3. Results

Out of the 48 line profiles obtained, 38 show double components and 10 show triple components which imply regions of complex kinematics. The expansion velocity was obtained for all the double component profiles as half of the relative velocity between the two components. Table 1 shows for all the double component line profiles, the  $v_{exp}$  with their corresponding

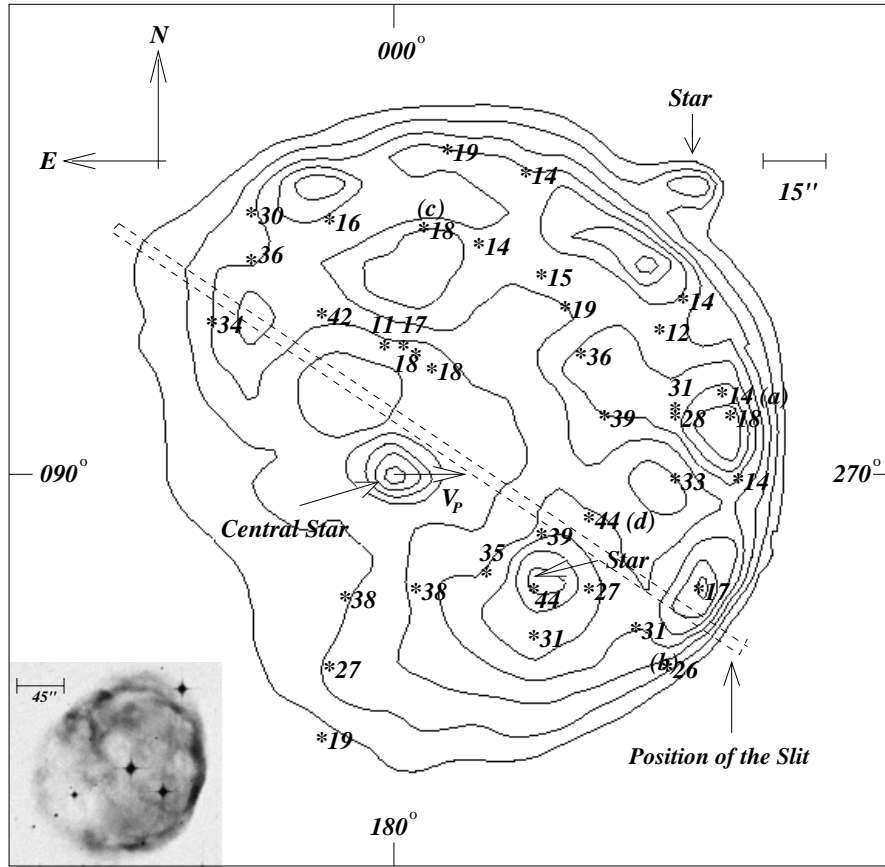


**Fig. 2.** Expansion velocity map of NGC 246 superimposed on the iso-intensity contour map in the [OIII] line. The stars indicate the central positions of the spatial segments and the numbers nearby them are the expansion velocities in km/s. The PA is measured from north to east with the central star as the origin (shown along the border at  $0^\circ$ ,  $90^\circ$ ,  $180^\circ$  and  $270^\circ$ ).  $V_p$  represents the direction of the proper motion. The values identified by *a*, *b*, *c*, *d* correspond to the profiles shown in Fig. 1.

representative spatial extents on the nebula ( $2.2'' \times \Omega''$ ). The individual Gaussian parameters for the blue-shifted (peak  $I_1$ , width  $W_1$ ) and red-shifted (peak  $I_2$ , width  $W_2$ ) components are also listed in the table. Fig. 1 shows a sample of four typical line profiles.

Fig. 2 shows a plot of  $v_{exp}$  at different positions on the nebula superposed on the iso-intensity contours obtained from the [OIII] line filtergram. Also shown in the figure are the POSS image of NGC 246 and the orientation of the spectrograph slit across the nebula. The positions corresponding to the profiles shown in Fig. 1 are also indicated in Fig. 2 (*a*, *b*, *c*, *d*). We can see from Fig. 2 that the spatial gradient of  $v_{exp}$  in the leading section is significantly steeper than that in the trailing section although we do not have adequate number of observing points in that section due to its intrinsic faintness. In Fig. 3, we have plotted the  $v_{exp}$  as a function of radial distance from the central star for various PAs in the leading (Fig. 3a) and the trailing (Fig. 3b) halves. As our observations could not cover the region on the central star of the PN, we take the value there as 38 km/s (Robinson et al. 1982; Weinberger 1989). In spite of the fact that the  $v_{exp}$  were space-averaged over varying extents, there is a significant consistency in our results, showing a steeper gradient in the leading edge than in the trailing edge.

The interstellar extinction coefficient  $c$  was calculated from the observed  $H\alpha$  and  $H\beta$  flux ratio. The absolute  $H\alpha$  and  $H\beta$  fluxes needed for this calculation were taken from Pottasch (1984) for a nebular temperature of  $\sim 10,000\text{K}$ . Assuming a

*Case B* condition, we calculate the value of  $c$  as  $0.34 \pm 0.03$ . The value of  $E_{B-V}$  calculated from  $c$  is  $0.21 \pm 0.02$  which is larger than the value calculated from Balmer decrement (0.0, Pottasch 1984). The observed spectra were de-reddened for the value of  $c$  and are shown in Fig. 4, extracted from the slit in two segments corresponding to the leading and the trailing halves of the nebula in order to find the difference, if any, in the electron temperature. Table 2 shows the observed and the de-reddened strengths of some of the most prominent lines (relative to  $H\beta = 100$ ) obtained for the two halves. The electron temperatures were derived from the [OIII] line intensities using the relation given by McKenna et al. (1996). Due to the marginal detection of the [OII] lines, accurate density determination could not be done.

#### 4. Discussion

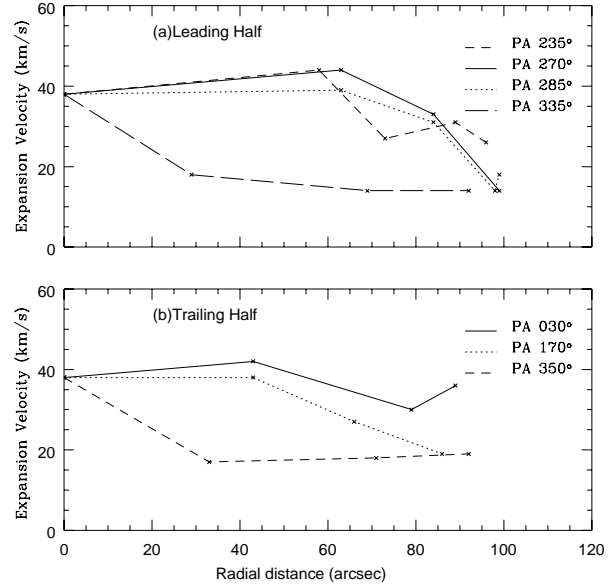
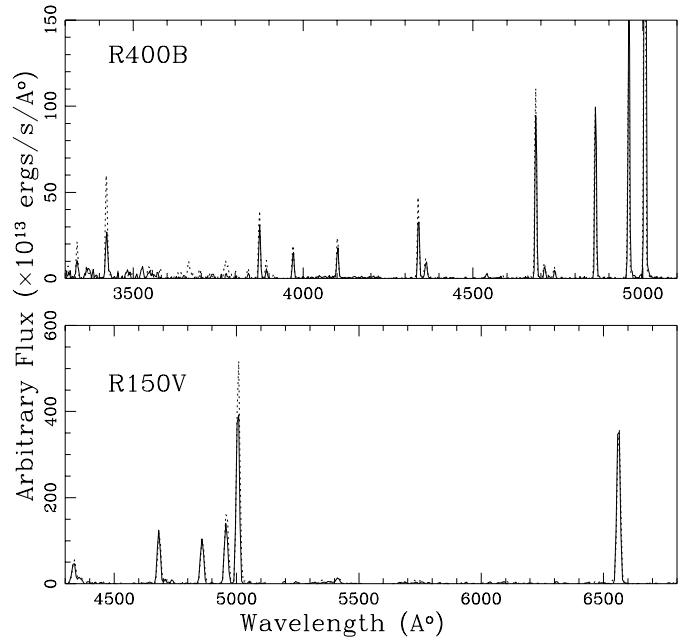
One of the best observable manifestations of the line of sight effects in a spherically symmetric PN is the gradual decrease of the central  $v_{exp}$  with radial distance by a factor  $\cos \theta$  where  $\theta$  is the angle between the line of sight and the radial direction at a given point on the sky-projected nebular image assuming a constant  $v_{exp}$ . We expect then,  $v_{exp}$  at the edge of NGC 246 to be 19 km/s. However, we observe a value of  $14 \pm 2$  km/s at the leading edge at the PA of  $270^\circ$  which is marginally lower than expected and at the trailing edge,  $19 \pm 2$  km/s (at the PA  $172^\circ$ ), which is as expected (Figs. 2 and 3). We attribute the decrease

**Table 1.** Line profiles parameters (see text for details)

$PA$ ( $^{\circ}$ )	$R$ ( $''$ )	$v_{exp}$ (km/s)	$W_1/W_2$	$I_1/I_2$	Sp.integ. ( $2'' \times \Omega''$ )
000	31	11	19/70	0.35/0.59	8
017	72	16	38/27	0.88/0.79	15
025	43	42	77/54	0.98/0.37	18
030	79	30	46/55	0.97/0.82	31
035	89	36	69/97	0.94/0.38	20
053	63	34	63/59	0.86/0.37	15
172	43	38	46/62	0.33/1.00	15
172	66	27	82/53	0.33/0.84	20
172	86	19	60/26	0.77/0.72	24
196	43	38	35/61	0.60/0.91	15
220	69	31	68/34	0.92/0.63	20
224	46	35	62/48	0.97/0.67	15
234	96	26	53/47	0.55/0.98	31
235	58	44	40/47	0.93/0.64	18
236	89	31	51/62	0.38/1.00	24
238	73	27	55/43	0.69/0.94	20
250	50	39	63/59	0.83/0.91	15
250	98	17	49/41	0.60/0.78	31
264	63	44	40/47	0.93/0.64	18
271	84	33	57/32	0.93/0.73	25
273	99	14	51/56	0.25/0.90	31
280	99	18	42/46	0.66/0.92	31
282	84	28	41/56	0.97/0.33	25
284	84	31	64/54	1.00/0.30	20
284	98	14	83/27	0.83/0.34	24
285	63	39	42/50	0.90/0.33	18
296	82	31	–	–	–
299	–	–	–	–	–
308	98	14	27/31	0.88/0.56	31
313	68	19	39/41	0.40/0.98	15
326	68	15	44/38	0.74/0.78	15
333	29	18	26/84	0.65/0.32	8
337	69	14	34/27	0.98/0.46	15
337	92	14	36/38	0.84/0.42	20
342	30	18	30/29	0.82/0.51	8
350	33	17	41/29	0.86/0.52	8
350	71	18	34/43	0.95/0.33	15
350	92	19	41/44	0.27/1.03	20

**Table 2.** Emission line intensities of the spectra;  $I_l, I_t$  are the observed and  $E_l, E_t$  are the de-reddened line intensities corresponding to the leading and trailing sections. The uncertainty in measuring the intensities of these lines varies from 1.5% to 6.9% of  $H\beta$ , with an average value of 3.9%.

Wave length ( $\text{\AA}$ )	$I_l/I_{l,H\beta}$	$E_l/E_{l,H\beta}$	$I_t/I_{t,H\beta}$	$E_t/E_{t,H\beta}$
4340 ( $H\gamma$ )	45	50	31	39
4363 ([OIII])	18	15	11	11
4686 (He II)	109	112	93	96
4863 ( $H\beta$ )	100	100	100	100
4959 ([OIII])	119	121	164	168
5007 ([OIII])	356	362	489	502
6563 ( $H\alpha$ )	374	296	361	307

**Fig. 3a and b.** Variation of  $v_{exp}$  with radial distance from the central star in **a** the leading and **b** the trailing halves. Notice that the spatial gradient of  $v_{exp}$  is considerably steeper in the leading edge than in the trailing edge.**Fig. 4.** IDS spectra of NGC 246. Solid curves represent the leading half and the dotted ones represent the trailing half.

in  $v_{exp}$  to the deceleration effect caused by the interaction of the PN with the ISM. We find (Fig. 3) that the gradient in the region of 60 – 90 arcsec from the central star for the leading edge is comparatively larger than in the trailing edge ( $0.9 \pm 0.13$  and  $0.3 \pm 0.13$  km/s/arcsec respectively). This suggests a deceleration effect on the leading section. We believe that this is the first time that a kinematic effect of the interaction has been reported. Further, the average width of the line profiles is found to be  $46 \pm 11$  km/s, excluding 10 profiles whose components have

large differences in their widths. The observed line widths can have contributions in general from (i) the thermal broadening, (ii) the turbulent broadening, (iii) the instrumental broadening and (iv) the broadening due to the radial dependent nebular expansion. However, the major contribution to the large widths (46 km/s) comes from the radial dependent expansion of the nebula as verified with a synthetically generated profile using a code. We notice that the profiles having components of nearly equal widths fall only on the voids. Seven out of the ten profiles with large difference in widths of the components come from higher density regions. Most of these components having larger widths also have larger amplitudes. The profiles with stronger blue components (larger value of  $I_1$  than  $I_2$  listed in Table 1) are concentrated more towards the high density regions; whereas, those with stronger red components are concentrated towards the voids. Although there are a few exceptions, the stronger blue components from the clumpy regions may be interpreted as due to the negative radial velocity of the nebula itself, assuming that the clumps are a result of the ISM interaction. Large expansions were found only in the voids and blobs show a lower expansion. The decrease of  $v_{exp}$  at positions where the nebular density is large can be understood as simply due to the momentum conservation. Further, the clumpy structures present in the edges of the nebula might have been caused by RT and KH instabilities (Dgani & Soker 1998).

From the IDS data we find that the electron temperature in the leading half is significantly larger ( $T_l = 2.4 \times 10^4$  K) than that in the trailing half ( $T_t = 1.56 \times 10^4$  K) with an average nebular temperature of  $1.98 \times 10^4$  K which is in good agreement with the value reported by Kaler (1983). We attribute this to the compression of the nebular shell by the ISM ram pressure. Assuming that the trailing half is not affected by the ISM interaction and that the compressional energy released in the leading half is not lost by radiative processes, we derive below a theoretical relation to find the temperature difference in the two halves.

Let us consider a cell of unit volume near the leading edge which is initially (before it significantly interacted with ISM) at the temperature of the undisturbed trailing half. Assuming that the ISM compresses the shell only in the radial direction, let  $\delta R'$  be the thickness of the compressed region of the leading half. From our filtergram we find  $\delta R \sim \delta R'$ . By considering the energy conservation, the internal kinetic energies of the cell before and after the compression ( $E_t$  &  $E_l$ ) are related as  $E_l = E_t + PdV$  where,  $P$  is the ISM ram pressure ( $= \rho_0[V_* + V_{exp}]^2$ ) which is assumed to be constant during the interaction, and  $dV$  is the change in the volume of the unit cell which is  $[1 - \delta R/(\delta R + \delta R')]$ . From this we arrive at the following relation for the difference in temperature,

$$T_l - T_t = \frac{2\mu n_0 m_H (V_* + V_{exp})^2}{3kn_n} \left[1 - \frac{\delta R}{(\delta R + \delta R')}\right] \cos\phi \quad (1)$$

where,  $k$  is the Boltzmann's constant,  $m_H$  is the mass of the hydrogen atom and  $\mu$  is the mean molecular weight ( $\sim 0.5$ , for a fully ionized hydrogen gas) and  $\phi$  is the angle between the slit position and the direction of proper motion ( $=45^\circ$ ). The

value of  $n_n$  is taken as the electron density in the leading edge which was estimated to be  $\sim 200 \text{ cm}^{-3}$  by Heap (1975). Taking the observed value of  $T_t$ , we get from the above relation,  $T_l = 2.6 - 2.1 \times 10^4$  K. The ISM density has been taken as  $5-10 \text{ cm}^{-3}$  (Soker et al. 1991). This is in good agreement with the value found from our observations.

## 5. Conclusions

1. From our spatio-kinematic study on NGC 246, we find a marginal evidence for the effect of the PN shell deceleration due to its interaction with the ISM.
2. The [OIII] electron temperature for the leading edge is found to be 1.54 times larger than that of the trailing edge from our spectrographic observations. We explain this effect in terms of the compression of the nebular shell by the ISM and calculate the temperature increment which is in good agreement with the value found from our observations.

*Acknowledgements.* This work was supported by the Department of Space, Government of India. The INT is operated on the island of La Palma by the Isaac Newton Group in the Spanish Observatorio del Roque de los Muchachos of the Instituto de Astrofísica de Canarias. We are grateful to the service manager Stephen Smartt for helping us in downloading the data. We thank R.T Patel for his help during Mt. Abu observations. We thank the anonymous referee for highly constructive comments.

## References

- Acker A., Ochsenbein F., Sterholm B., et al. 1992, ESO-Strasbourg Catalog of Planetary Nebulae
- Acker A., Fresneau A., Pottasch S.R., et al. 1998 A&A 337, 253
- Anandarao B.G., Rao S.R., 1985, BASI 14, 25
- Atherton P.D., Taylor K., Pike C.D., et al., 1982, MNRAS 201, 661
- Borkowski J., Sarazin L., Soker N., 1990, ApJ 360, 173
- Chakraborty A., Anandarao B.G., 1997, AJ 114, 1576
- Chu Y.H., Jacoby G.H., Arendt R., 1987, ApJSS 64, 529
- Dgani R., Soker N., 1998, ApJ 495, 337
- Gurzadyan G.A., 1969, Planetary Nebulae (Gordon and Breach, New York), 235
- Heap S.R., 1975, ApJ 196, 195
- Hollis J.M., Buren D.V., Vogel S.N., 1996, ApJ 456, 644
- Johnson H.M., 1976, ApJ 208, 127
- Joncas G., Roy J.R., 1986, ApJ 309, 649
- Kaler J.B., 1983, ApJ 271, 188
- McKenna F.C., Keenan F.P., Kaler J.B., et al., 1996, PASP 610, 614
- Philip P., Soker N., 1990, AJ 99, 1883
- Pottasch S.R., 1984, Planetary Nebulae (Dordrecht: Reidel)
- Pottasch S.R., 1996, A&A 307, 561
- Robinson G.J., Reay N.K., Atherton P.D., 1982, MNRAS 199, 649
- Sabbadin F., Strafella F., Bianchini A., 1986, A&AS 65, 259
- Schneider S.E., Terzian Y., Purgathofar A., et al., 1983, ApJSS 52, 399
- Seema P., Anandarao B.G., Banerjee D.P.K., et al., 1992, PASP 104, 1091
- Soker N., Borkowski J., Sarazin L., 1991, AJ 102, 1381
- Soker N., Zucker D.B., 1997, MNRAS 289, 665
- Tweedy R.W., Martos M.A., Noriega-Crespo A., 1995, ApJ 445, 257
- Vaughan J.M., 1989, The Fabry – Perot interferometers, (Adam Hilger, Bristol)
- Weinberger R., 1989, AASS 78, 301